High-resolution velocity spectra using eigenstructure methods

Biondo Biondi and Clement Kostov

ABSTRACT

Stacking velocity analysis provides optimal estimates for the parameters of a few, well separated reflections in additive white noise. To resolve close, interfering reflections, we adapt a theory developed originally for radar and sonar applications to the particular reflection seismics experiment. In seismic data the wavefronts are wide-band and the curvature of the wavefronts is significant across the receivers array. We introduce a family of estimators for the wavefront parameters based on the eigenstructure of the data covariance matrix. The traditional stacking method can be related to the new high-resolution estimators and the superiority of the latter is explained with a simple geometric construction.

A field-data example shows that the high resolution estimators are particularly attractive for local spectra estimation where short arrays are considered. Several realistic synthetic examples illustrate the new method and show its superiority in estimating stacking velocity spectra.

INTRODUCTION

The estimation of stacking velocities is a classic problem in exploration seismology. A related problem is the estimation of the ray parameter of a plane wave. Both problems are particular cases of the more general problem of estimating the wavefront shape of a signal recorded by a linear array of receivers. In the near field, the wavefront is hyperbolic, and therefore is conveniently parametrized by stacking velocity. In the far field, the wavefront is well approximated by plane waves that can be described by ray parameters. From now on we will use the general term shape parameter to indicate both velocity and ray parameter.

The standard solution to the estimation of stacking velocities is to pick the maxima of shape-parameter spectra (Taner and Koehler, 1969). The spectra are

computed by repeating, for a sweep of shape parameters, a time correction that aligns the wavefront in space along the array, and a coherency measure along the spatial direction. The time correction could be normal moveout (NMO) or linear moveout (LMO). The coherency measure could be simple stacking or the computation of a semblance function.

The stacking spectrum, and in particular the velocity spectrum, has many attractive properties. It yields the maximum-likelihood estimates of the shape-parameter when the statistics of the data are Gaussian and there is only one wavefront impinging on the array. Further, the estimate is robust with respect to deviations of the data from the assumed simple propagation model or from Gaussian statistics. When two or more wavefronts impinge on the array the classical procedure still yields good estimates of their shape parameters, provided the wavefront shapes are sufficiently different.

Poor resolution is the main disadvantage of the stacking spectrum. When a pair of wavefronts are too close, the resulting estimates are biased. Even worse, the spectra show only one maximum and indicate only one wavefront impinging on the array. In reflection seismology, the stacking spectra fail typically to separate interfering events at later times and higher velocities. In many interesting situations, higher resolution spectra are needed to resolve reflection events, for instance primaries from reflectors with conflicting dips, or a primary and an intrabed or peg-leg multiple.

High-resolution spectra can be even more useful in the estimation of local spectra such as local slant stacks (Sword, 1987) or beam stacks (Kostov and Biondi, 1987). Local spectra have two advantages over conventional methods (1) the physical model describing the data is more accurate, for instance the plane wave approximation is appropriate only in the Fresnel zone, and (2) they are more sensitive to small scale variations of the shape parameter. On the other hand local spectra have poorer resolution because they are estimated from shorter arrays. This limitation can be compensated using high resolution methods.

Many algorithms have been developed, in particular for sonar and radar applications, for increasing the resolution of wavefront shape estimation. They are called *adaptive* algorithms because they "adapt" to the data using the information yielded by an estimate of the data covariance matrix. The main reason why these new methods show an improvement in resolution is that the interfering wavefronts are properly included in the data model and not treated as spatially incoherent noise as in the usual stacking spectrum. Among the adaptive methods, the algorithms based on the eigenstructure of the covariance matrix of the data are particularly interesting for their performances (Bienvenu and Kopp, 1983) (Schmidt, 1986). These algorithms were first derived for the case of narrow-band signals and have been generalized later to the case of wide-band signals (Wax et al., 1984)(Wang and Kaveh, 1985). The application of the high resolution methods to seismic reflections is more complicated than their application to sonar or radar data, because the seismic data

are both wide-band and highly non-stationary, in the sense that the shape parameter of the reflections can vary rapidly with time. Therefore only few time samples can be used for the estimation of the covariance matrix, yielding poor estimates of the covariance matrix itself.

In the first section we present the eigenstructure algorithms applied to narrow-band signals. Then we compare the new methods with the classical stacking method and show a geometric explanation for the superiority of the former. The third section contains an extension of the narrow-band method to the general case of a wide-band signal. In this section we discuss the particular features of the seismic problem and the trade-off between resolution and robustness in the application of the method to the seismic signal. The last two sections illustrate with a field-data example and some synthetic examples the applications of the high-resolution methods to seismic velocity analysis and local slant stacks.

THE NARROW-BAND CASE

The recorded data are assumed to be complex and narrow-band, with central angular pulsation ω. The seismic signal is real, but it can be easily transformed in an analytical signal using the Hilbert transform (Claerbout, 1976). Some advantages of working with the analytical signal, rather than with the real-valued one, are discussed by Sguazzero and Vesnaver, 1987. The data recorded at the M receivers are described as the combination of W wavefronts and additive noise. The model for the data recorded by the receiver m at time t is

$$d(m,t) = \sum_{w=1}^{W} s_w(t - \tau_w(m;\theta_w)) \quad + \quad n(m,t), \tag{1}$$

where $n(t,m)$ is the additive noise, assumed to be uncorrelated with the sources $s_w(t)$. The delays of arrival of the wavefronts at the receiver m with respect to zero-offset travel time τ_0 are denoted by and $\tau_w(m;\theta_w)$. When the wavefronts are plane waves, the delays are expressed as

$$\tau_w(m;\theta_w) = \theta_w \Delta x(m-1), \tag{2}$$

where Δx is the spacing between the receivers and θ_w the ray parameter of the w wavefront. When the wavefront shapes are hyperbolic, the delays are

$$\tau_w(m;\theta_w) = \sqrt{\tau_0^2 + \theta_w^2(\Delta x(m-1))^2} - \tau_0, \tag{3}$$

where now θ_w is the RMS slowness. The sources $s_w(t)$ are modeled as narrow-band stochastic processes. Thus the time shifts are complex exponentials and the data can be expressed as

$$d(m,t) = \sum_{w=1}^{W} s_w(t)\, e^{j\omega\tau_w(m;\theta_w)} + n(m,t) d(m,t) = \sum_{w=1}^{W} \sqrt{M} s_w(t)\, \frac{e^{j\omega\tau_w(m;\theta_w)}}{\sqrt{M}} + n(m,t). \tag{4}$$

The recorded data are truncated and a segment of T time samples, centered at τ_0, is windowed. In matrix notation the data are expressed as

$$\mathbf{D} = \mathbf{A}(\Theta)\mathbf{S} + \mathbf{N}, \tag{5}$$

where $\mathbf{D}$ and $\mathbf{N}$ are $(M \times T)$ data and noise matrices. $\mathbf{S}$ is a $(W \times T)$ source matrix and $\mathbf{A}(\Theta)$ is the *steering matrix* function of the vector of parameters Θ. The steering matrix is a $(M \times W)$ matrix formed by the W *steering vectors* $\mathbf{a}_w(\theta_w)$

$$\mathbf{a}_w(\theta_w) = \frac{1}{\sqrt{M}} \begin{pmatrix} e^{j\omega\tau_w(1;\theta_w)} \\ \cdot \\ \cdot \\ e^{j\omega\tau_w(m;\theta_w)} \\ \cdot \\ \cdot \\ e^{j\omega\tau_w(M;\theta_w)} \end{pmatrix}. \tag{6}$$

The sources are assumed to be zero-mean stochastic processes and uncorrelated with the noise. The data covariance matrix is therefore

$$\mathbf{R}_d = E[\mathbf{D}\mathbf{D}^H] = \mathbf{A}(\Theta)E[\mathbf{S}\mathbf{S}^H]\mathbf{A}(\Theta)^H + \mathbf{R}_n = \mathbf{A}(\Theta)\mathbf{R}_s\mathbf{A}(\Theta)^H + \mathbf{R}_n, \tag{7}$$

where $\mathbf{R}_s$ and $\mathbf{R}_n$ are the respective covariance matrices, of the sources and the noise.

For simplicity we will assume that the noise is spatially uncorrelated, with equal power for all the receivers. Equation (7) becomes then

$$\mathbf{R}_d = \mathbf{A}(\Theta)\mathbf{R}_s\mathbf{A}(\Theta)^H + \sigma_n^2\mathbf{I}. \tag{8}$$

The above assumption about the noise statistics does not limit the generality of the method, because if $\mathbf{R}_n$ were known the data could either be prewhitened (Bienvenue and Kopp, 1983) or the eigenstructure of the positive definite matrix pencil $(\mathbf{R}_d, \mathbf{R}_n)$ could be used (Schmidt, 1986).

Properties of the eigenstructure of the data covariance matrix

When the sources' covariance matrix $\mathbf{R}_s$ is not singular, i.e. there are neither pairs of fully correlated sources nor linearly dependent steering vectors $\mathbf{a}_w(\theta_w)$, the matrices $\mathbf{R}_s$, and $\mathbf{A}(\Theta)$ have rank W (here we assume that $M \geq W$), and therefore also the matrix $\mathbf{A}(\Theta)\mathbf{R}_s\mathbf{A}(\Theta)^H$ has rank W.

Let $[\lambda_1 \geq \lambda 2 \ldots \geq \lambda_M]$ be the eigenvalues, and let $[\mathbf{E}_1, \mathbf{E}_2, \ldots . \mathbf{E}_M]$ be the eigenvectors of the data covariance matrix $\mathbf{R}_d$. Equation (8) implies that the eigenvalues of $\mathbf{R}_d$ are of the form $\lambda = \mu + {\sigma_n}^2$, with μ eigenvalue of $\mathbf{A}(\Theta)\mathbf{R}_s\mathbf{A}(\Theta)^H$, and therefore μ is positive. Having established that the rank of $\mathbf{R}_s$ is W, the two following properties hold:

1) The minimal eigenvalue is σ_n with multiplicity $M - W$. That is:

$$\lambda_{W+1} = \lambda_{W+2} = ... = \lambda_M = \sigma_n^2 \tag{9a}$$

2) The eigenvectors corresponding to the minimal eigenvalues are orthogonal to the data steering vectors $\mathbf{a}_w(\theta_w)$. That is:

$$\mathbf{a}_w(\theta_w)^H \mathbf{E}_m = 0 \qquad m = W+1, W+2, ..., M. \tag{9b}$$

The subspace $\mathbf{E}_n = [\mathbf{E}_{W+1}, \mathbf{E}_{W+2}, ..., \mathbf{E}_M]$ spanned by the eigenvectors corresponding to the minimal eigenvalues is called the *noise subspace.* The noise subspace is orthogonal to the *signal subspace* $\mathbf{E}_s = [\mathbf{E}_1, \mathbf{E}_2, ..., \mathbf{E}_W]$ that coincides with the subspace spanned by the data steering vectors $\mathbf{a}_w(\theta_w)$.

The first property is used to determine the number of wavefronts impinging on the array. The second property is used to estimate the wavefront shapes.

Determination of the number of wavefronts

In practice, the data covariance matrix is unknown and must be estimated from the recorded data. The maximum likelihood estimate of the covariance matrix is

$$\hat{\mathbf{R}}_d = \frac{1}{T}\ \mathbf{D}\mathbf{D}^H. \tag{10}$$

Property 1) in Equation (9a) does not hold exactly for the eigenvalues $[\hat{\lambda}_1 \geq \hat{\lambda}2 \ ... \ \geq \hat{\lambda}_M]$ of the estimated data covariance matrix $\hat{\mathbf{R}}_d$. In general the lowest $M - W$ eigenvalues are different. Therefore, determining the number of wavefronts requires a decision based on a statistical criterion.

Wax and Kailath (1985) have proposed two criteria to determine the number of wavefronts. Their criteria are similar to the ones introduced by Akaike (1973) and Rissanen (1978) for model selection in system identification. These criteria minimize the difference between (1) the log-likelihood function of the maximum likelihood estimator of the number of parameters in the model, and (2) a term penalizing overparametrization of the model.

The Akaike criterion (AIC) minimizes the function

$$AIC(W) = -2 \log \left(\frac{\prod_{m=W+1}^{M} \hat{\lambda}_m^{1/(M-W)}}{\frac{1}{M-W} \sum_{m=W+1}^{M} \hat{\lambda}_m} \right)^{(M-W)T} + \ 2W(2M - W). \tag{11}$$

The Rissanen criterion, called also minimum descriptive length (MDL) criterion, minimizes the function

$$MDL(W) = -2\log\left(\frac{\prod_{m=W+1}^{M}\hat{\lambda}_m^{1/(M-W)}}{\frac{1}{M-W}\sum_{m=W+1}^{M}\hat{\lambda}_m}\right)^{(M-W)T} + W(2M-W)\log(T). \quad (12)$$

The two criteria yield the same estimate of the number of wavefronts in most practical situations. The MDL criterion has the theoretical advantage of yielding a consistent estimate of the number of wavefronts, while the AIC tends, asymptotically, to overestimate the number of signals.

In practice, both criteria tend to overestimate the number of signals when few time samples are used in the estimate of the covariance matrix. In seismic applications it is seldom interesting to detect more than two or three interfering wavefronts; it is therefore recommended to set a low limit, two or three, for the maximum number of wavefronts W.

Estimation of the wavefront-shape parameters

Property 2 in Equation (9b) ensures that the data steering vectors $a_w(\theta_w)$ are orthogonal to the noise subspace $\mathbf{E}_n$, and consequently, that they belong to the signal subspace. If $\mathbf{a}(\theta)$ is the continuum described by the steering vectors for all the θ, $\hat{\theta}$ is a solution of the estimation problem if $\mathbf{a}(\hat{\theta})$ belongs to the signal subspace $\mathbf{E}_s$. The solution is unique when only W vectors in $\mathbf{a}(\theta)$ belong to $\mathbf{E}_s$. A sufficient condition for uniqueness is that any set of $W+1$ steering vectors are linearly independent. Further, a set of different shape parameters implies linearly independent steering vectors when the signal is not aliased, i.e. the spacing between the receivers is smaller than the half-wavelength of the signal.

In practice, the signal and the noise subspace are unknowns to be estimated from $\hat{\mathbf{R}}_d$. Once the number of wavefronts is determined, the maximum likelihood estimates of the signal and noise subspaces are, respectively, $\hat{\mathbf{E}}_s = [\hat{\mathbf{E}}_1, \hat{\mathbf{E}}_2, ...\hat{\mathbf{E}}_W]$, and $\hat{\mathbf{E}}_n = [\hat{\mathbf{E}}_{W+1}, \hat{\mathbf{E}}_{W+2}, ..., \hat{\mathbf{E}}_M]$, where the $\hat{\mathbf{E}}_m$ are the eigenvectors of $\hat{\mathbf{R}}_d$ (Anderson, 1963). The shape-parameter spectrum can be computed for every θ by measuring the closeness of the steering vector $\mathbf{a}(\theta)$ to the estimated signal subspace $\hat{\mathbf{E}}_s$, or by measuring its orthogonality to the estimated noise subspace $\hat{\mathbf{E}}_n$. Three equivalent expressions for the shape-parameter spectrum are:

$$P_{s1}(\theta) = \sum_{m=1}^{W} \mid \mathbf{a}(\theta)^H \hat{\mathbf{E}}_m \mid^2, \quad (13a)$$

and

$$P_{s2}(\theta) = \frac{1}{1 - \sum_{m=1}^{W} \mid \mathbf{a}(\theta)^H \hat{\mathbf{E}}_m \mid^2} \quad (13b)$$

when using the signal subspace, or

$$P_{n1}(\theta) = \frac{1}{\sum_{m=W+1}^{M} \mid \mathbf{a}(\theta)^H \hat{\mathbf{E}}_m \mid^2} \tag{13c}$$

when using the noise subspace. $P_{s2}(\theta)$ and $P_{n1}(\theta)$ yield exactly the same spectrum, while $P_{s1}(\theta)$ has the same maxima of the others, and therefore is equivalent for the estimation of the shape parameter θ.

Another useful shape-parameter spectrum is

$$P_{n2}(\theta) = \frac{1}{\sum_{m=W+1}^{M} \frac{1}{\hat{\lambda}_m} \mid \mathbf{a}(\theta)^H \hat{\mathbf{E}}_m \mid^2}. \tag{14}$$

In general, the maxima of $P_{n2}(\theta)$ are different from the maxima of $P_{n1}(\theta)$. $P_{n2}(\theta)$ usually yields better estimates when the number of time samples T is small.

Correlated sources and spatial smoothing

The only assumption of the high-resolution velocity analysis methods presented above that would be unrealistic for seismic data is the lack of correlation between the sources of the interfering wavefronts. When the interfering wavefronts are a primary and a multiple, their waveforms are probably highly correlated.

If two sources are fully correlated the source covariance matrix $\mathbf{R}_s$ is singular, and therefore, the properties in Equations (9) do not hold any more. In practice, even two highly, but not fully-correlated sources could be unresolvable by eigenstructure velocity analysis.

An effective method to *uncorrelate* the sources of signal before applying the eigenstructure method, is to apply *spatial smoothing* while estimating the covariance matrix from the data (Shan et al., 1985) (Shan et al., 1987). Spatial smoothing increases the rank of the source covariance matrix $\mathbf{R}_s$.

The original array of M receivers is divided into K overlapping subarrays of $(M - K + 1)$ receivers, as shown in Figure 1. The covariance matrix $\mathbf{R}_d^k$ can be defined for each subarray k, and the *spatially smoothed* covariance matrix is defined as

$$\hat{\mathbf{R}}_d^K = \frac{1}{K} \sum_{k=1}^{K} \hat{\mathbf{R}}_d^k. \tag{15}$$

When the wavefronts have linear delays, i.e. they are plane waves incident on a uniform array, it can be shown first that the steering vector matrices are related to each other by

$$\mathbf{A}^k(\Theta) = \mathbf{A}^{k-1}(\Theta) diag(e^{j\Delta x}) = \mathbf{A}(\Theta) diag(e^{j(k-1)\Delta x}),$$

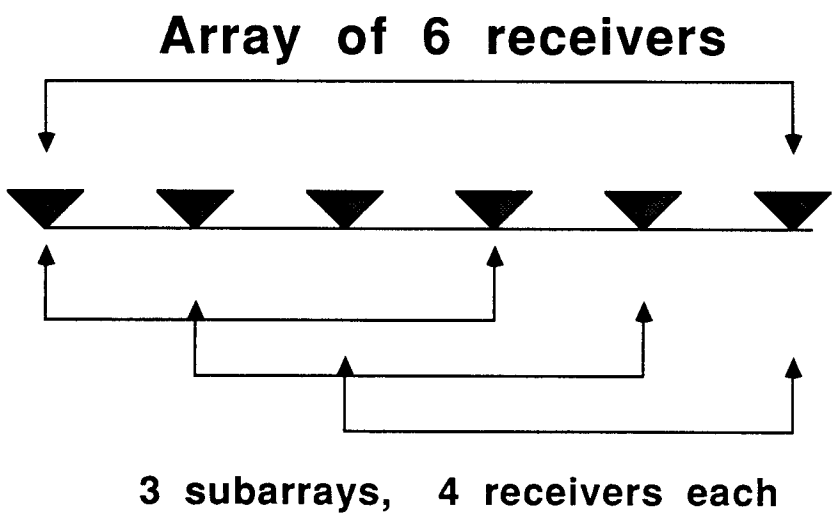

FIG. 1. Subdivision of the original array of M receivers in K subarrays of $M-K+1$ receivers for applying *spatial smoothing.*

and second, that $\mathbf{R}_d^K$ is equal to

$$\mathbf{R}_d^K = \frac{1}{K}\sum_{k=1}^{K}\mathbf{A}^k(\Theta)\mathbf{R}_s\mathbf{A}^k(\Theta)^H + \sigma_n^2\mathbf{I} = \mathbf{A}(\Theta)(\frac{1}{K}\sum_{k=1}^{K}\mathbf{R}_s^k)\mathbf{A}(\Theta)^H + \sigma_n^2\mathbf{I} =$$

$$\mathbf{A}(\Theta)\mathbf{R}_s^K\mathbf{A}(\Theta)^H + \sigma_n^2\mathbf{I}, \tag{16}$$

with $\mathbf{R}_s^K$ not singular when the number of subarrays K is greater than or equal to the number of wavefronts. When $\mathbf{R}_s^K$ is not singular the eigenstructure method can be applied to estimate the shape-parameters vector Θ.

Theoretically, the spatial smoothing technique cannot be applied unless the wavefronts are plane. The relations in equation (16) are not valid for nonplanar wavefronts, because the $\mathbf{A}^k(\Theta)$ are not simply related to $\mathbf{A}(\Theta)$. However, if the number of subarrays (K) is small, the relations in Equation (16) are still approximately true, and the spatial smoothing technique can be successfully applied.

Spatial smoothing reduces the effective aperture of the array from M to $(M - K + 1)$, and consequently, slightly reduces the resolution of the method.

COMPARISON WITH THE STACKING METHOD

In the narrow-band case, the shape-parameter spectrum computed using the classical method of time corrections followed by stacking, can also be expressed as a function of the covariance matrix of the data. The stack averaged over a temporal

window T time samples long is

$$Stack(\theta) = \frac{1}{T}\sum_{t=1}^{T}\frac{1}{M}\sum_{m=1}^{M} d(m, t + t_w(m)). \tag{17}$$

Time shifting is multiplication by a complex exponential; thus the stack can be expressed in matrix notation as

$$Stack(\theta) = \frac{1}{T}\sum_{t=1}^{T}(\mathbf{a}^H(\theta)\mathbf{D}). \tag{18}$$

The average of the squares of the absolute values of the stacks is the stacking spectrum

$$P_{Stack}(\theta) = \frac{1}{T}\mathbf{a}^H(\theta)\mathbf{D}\ \ (\mathbf{a}^H(\theta)\mathbf{D})^H = \frac{1}{T}\mathbf{a}^H(\theta)\mathbf{D}\mathbf{D}^H\mathbf{a}(\theta) =$$

$$\mathbf{a}(\theta)^H\ \hat{\mathbf{R}}_d\ \mathbf{a}(\theta). \tag{19}$$

The stacking spectrum, as a function of the eigenvalues and eigenvectors of the data covariance matrix, is

$$P_{Stack}(\theta) = \mathbf{a}(\theta)^H\ \hat{\mathbf{R}}_d\ \mathbf{a}(\theta) = \sum_{m=1}^{M} \hat{\lambda}_m |\ \mathbf{a}(\theta)^H\hat{\mathbf{E}}_m\ |^2. \tag{20}$$

Figure 2 shows a stacking spectrum for a monochromatic plane wave with frequency 25 Hz and ray parameter $\theta = .25$ s/Km. The array has 40 receivers spaced 10 m. When only one wavefront impinges on the array, the first eigenvector $\mathbf{E}_1$ of the data covariance matrix is the data steering vector $\mathbf{a}_1(\theta_1)$. The zeros in the spectrum correspond to steering vectors $\mathbf{a}(\theta)$ orthogonal to the first eigenvector; their spacing is $\Delta\theta = 2\pi/\omega M\Delta x$. The resolution limit of the stacking spectrum is of the order of the half-width of the main lobe, i.e. the spacing between the zeros $\Delta\theta$.

The stacking spectrum, Equation (20), differs from the eigenstructure spectrum, Equation (13a), in two ways. First, and most important, is the weighting by eigenvalues in the summation in Equation (20). The weights in equation (20) reward steering vectors close to eigenvectors corresponding to the largest eigenvalues. On the contrary the spectrum in Equation (13a) is a projection of the steering vectors on the signal subspace; it does not privilege any direction in this subspace. Second, the ranges of the summation differ. In the stacking method, the summation is carried over for all the eigenvectors. In the eigenstructure method, it is limited to the eigenvectors belonging to the signal subspace. Limiting the summation reduces the effects of the noise and of the finite number of time samples used in the estimation on the spectrum.

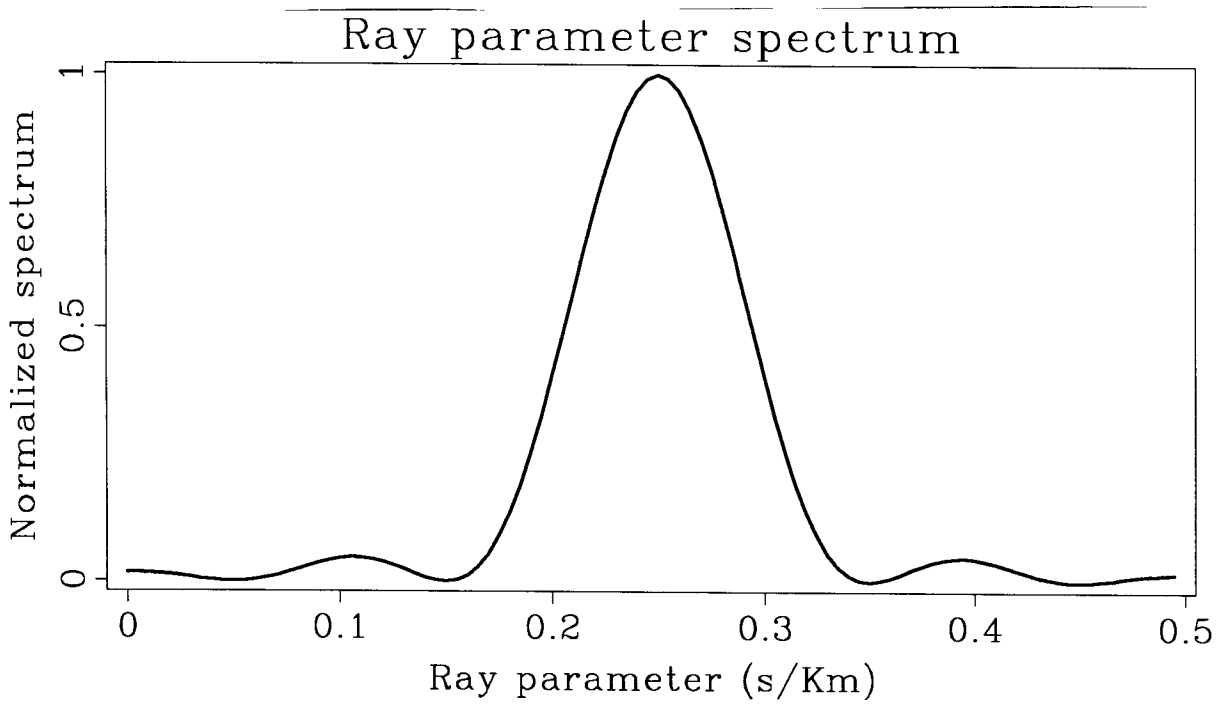

FIG. 2. Stacking spectrum for a monochromatic plane wave with frequency 25 Hz and ray parameter $\theta = .25$ s/Km. The array has 40 receivers spaced 10m. The distance between the zeros in the spectrum is $\Delta\theta = 2\pi/\omega M\Delta x$.

Geometric interpretation: uncorrelated sources

The superior resolution achieved by the eigenstructure spectrum can be easily explained by geometric considerations. In this section we consider the case of two plane waves, generated by uncorrelated sources with equal power, and noise-free receivers. The eigenvectors $\mathbf{E}_1$ and $\mathbf{E}_2$ shown in Figure 3, define the signal subspace in the (M+1)-dimensional vector space spanned by the (M+1) orthonormal steering vectors $[\mathbf{a}(\theta = 0), \mathbf{a}(\theta = \pm\Delta\theta)\mathbf{a}(\theta = \pm 2\Delta\theta), ..., \mathbf{a}(\theta = \pm\frac{M}{2}\Delta\theta)]$. The cosine of the angle α between the two data steering vectors is given by their dot product, assumed here to be a real quantity (for simplification of the algebra). The cosine of α is

$$\cos\alpha = \mathbf{a}_1(\theta_1)^H\mathbf{a}_2(\theta_2) = \frac{\sin(\omega\Delta x M((\theta_2-\theta_1)/2))}{M\sin(\omega\Delta x((\theta_2-\theta_1)/2))} = \frac{\sin(2M\beta)}{\sin(2\beta)}, \qquad (21)$$

with $\beta = \omega\Delta x(\theta_2 - \theta_1)/4$.

The eigenvalues of the data covariance matrix are

$$\lambda_1 = S(1+\cos\alpha), \quad \lambda_2 = S(1-\cos\alpha), \quad \text{and } \lambda_m = 0 \quad \text{for } m > 2. \qquad (22a)$$

The first two eigenvectors are

$$E_1 = \frac{\mathbf{a}_1(\theta) + \mathbf{a}_2(\theta)}{\sqrt{2+2\cos\alpha}} \quad \text{and} \quad \mathbf{E}_2 = \frac{\mathbf{a}_1(\theta) - \mathbf{a}_2(\theta)}{\sqrt{2-2\cos\alpha}} \qquad (22b)$$

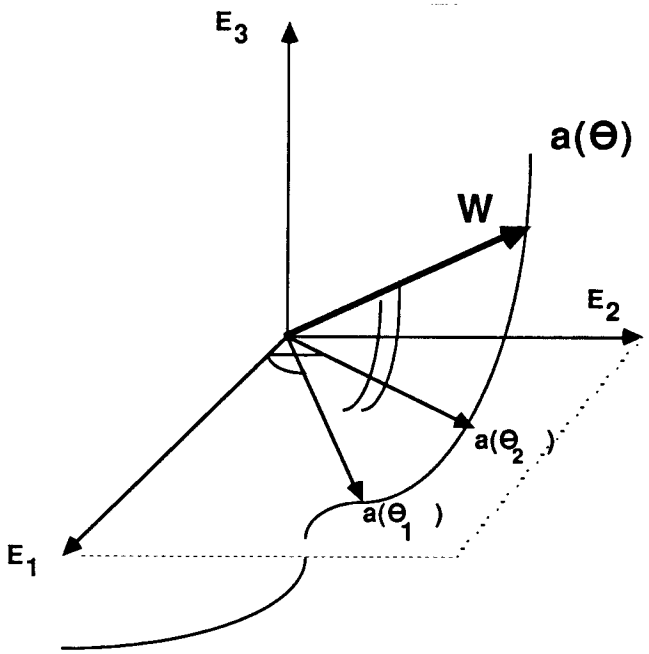

FIG. 3. Geometric interpretation of the stacking spectrum and of the eigenstructure spectrum in the case of two incident plane waves. The first two eigenvectors , $\mathbf{E}_1$ and $\mathbf{E}_2$, define the *signal subspace*. Vectors $\mathbf{a}_1$ and $\mathbf{a}_2$ are the data steering vectors. They lie in the *signal subspace*. The vector $\mathbf{w}$ belongs to the continuum $\mathbf{a}(\theta)$, but not to the signal subspace. When the angle α between the data steering vectors is too small, the stacking spectrum shows a maximum for $\mathbf{w}$ instead for $\mathbf{a}_1$ and $\mathbf{a}_2$.

The two eigenvectors $\mathbf{E}_1$ and $\mathbf{E}_2$ do not necessarily belong to the continuum $\mathbf{a}(\theta)$. Unless the data are spatially aliased, the continuum $\mathbf{a}(\theta)$ intersects the signal subspace only in $\mathbf{a}_1(\theta_1)$ and $\mathbf{a}_2(\theta_2)$. The eigenstructure spectrum in Equation (13a) is a projection of the steering vectors on the signal subspace; it thus has two maxima exactly in θ_1 and θ_2.

By contrast, the stacking spectrum has a spurious maximum at $(\theta_1+\theta_2)/2$. The steering vector $\mathbf{w}((\theta_1+\theta_2)/2)$ is out of the signal subspace but is close to the first eigenvector. The closer the two data steering vectors, the larger the first eigenvalue than the second, and the larger the weight given to the steering vector $\mathbf{w}((\theta_2+\theta_1)/2)$ in the summation (20) in comparison with the weights of the steering vectors $\mathbf{a}_1(\theta_1)$ and $\mathbf{a}_2(\theta_2)$.

Stacking spectra at $\theta=\theta_1=\theta_2$ and $\theta=(\theta_1+\theta_2)/2$ can be evaluated computing the appropriate dot products. The results are:

$$P_{Stack}(\theta_1)=P_{Stack}(\theta_2)=1+\cos^2(\alpha)=1+\frac{1}{M^2}\left[\frac{\cos(M\beta)\sin(M\beta)}{\cos(\beta)\sin(\beta)}\right]^2; \qquad (23)$$

and

$$P_{Stack}((\theta_1+\theta_2)/2)=\frac{2}{M^2}\left[\frac{\sin(M\beta)}{\sin(\beta)}\right]^2. \qquad (24)$$

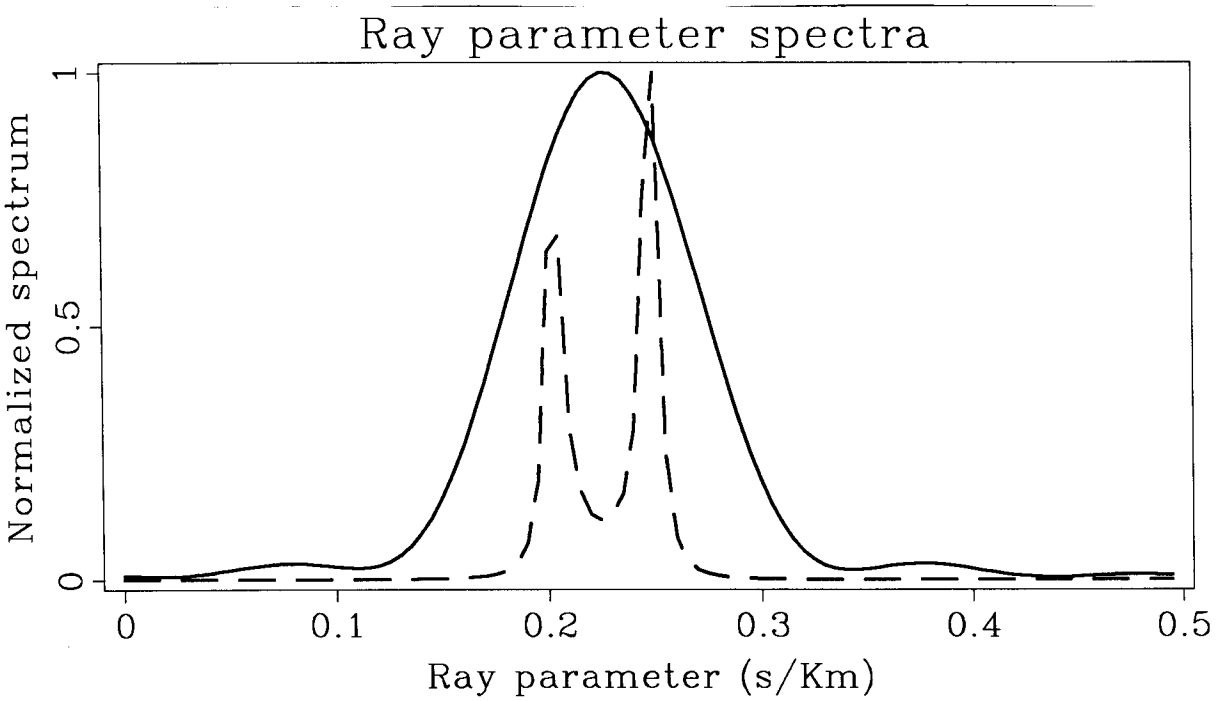

FIG. 4. Stacking spectrum (solid line) and eigenstructure spectrum (dashed line) for two monochromatic plane waves. The ray parameters are $\theta_1 = .2$ s/Km and $\theta_2 = .25$. The angle α between the two data steering vectors is 50°.

The ratio between the stacking powers at angles θ_1 and $(\theta_1 + \theta_2)/2$ can be approximated for small values of β in the following way:

$$\frac{P_{Stack}(\theta_1)}{P_{Stack}((\theta_1+\theta_2)/2)} \approx \frac{1-(M^2-1)\frac{\beta^2}{4}}{1-\frac{\beta^2}{2}} \leq 1.$$

This expression shows that the stacking power at $(\theta_1 + \theta_2)/2$ is larger than the stacking power at θ_1, when the angles θ_1 and θ_2 are close to each other. Therefore, when the two data steering vectors are too close, the stacking spectrum has a maximum in $(\theta_1 + \theta_2)/2$ instead of two maxima in θ_1 and θ_2.

Figure 4 shows a stacking spectrum (solid line) superimposed upon an eigenstructure spectrum (dashed line) computed, using Equation (13b). The two spectra are normalized to one. The data are two monochromatic plane waves with frequency 25 Hz, and ray parameters $\theta_1 = .2$ s/Km and $\theta_2 = .25$ s/Km. The array has 40 receivers spaced 10 m, the time sampling is 4 ms. With these parameters, the angle α between the two plane waves is about 50°. The stacking spectrum has not resolved the two plane waves and has a maximum at $(\theta_1 + \theta_2)/2$. The eigenstructure spectrum has resolved the two plane waves and has two maxima exactly at θ_1 and θ_2.

Geometric interpretation: correlated sources

When two plane waves are correlated they are more difficult to resolve both for the stacking spectrum and for the eigenstructure spectrum. If S_{12} is the diagonal term of the sources covariance matrix $\mathbf{R}_s$, assumed to be real, the eigenvalues of the data covariance matrix are:

$$\lambda_1 = (S + S_{12})(1 + \cos\alpha), \quad \lambda_2 = (S - S_{12})(1 - \cos\alpha), \quad \text{and} \quad \lambda_m = 0 \text{ for } m > 2, \quad (25)$$

while the eigenvectors are the same as for uncorrelated sources (Equation 22b).

The correlation between the sources decreases the *effective angle* between the data steering vectors. When the sources are fully correlated, only one eigenvalue is different from zero. Then the stacking method and the eigenstructure spectrum yield the same spectra.

Figure 5 shows a stacking spectrum (solid line) superimposed upon an eigenstructure spectrum (dashed line). The data are two monochromatic plane waves as in Figure 4, but now the waveforms are fully correlated. Neither method resolves the two correlated signals. On the other hand, applying spatial smoothing, as presented in the previous section, the eigenstructure method resolves the two wavefronts. Figure 6 shows the results when spatial smoothing is applied by dividing the original array in 11 subarrays. The spatially smoothed covariance matrix is used for the computation of both spectra.

In this section we considered the simple case of two plane waves and noiseless data. We did not consider the effect of the limited data on the quality of the estimate of the data covariance matrix. The reader interested in a more general discussion of the statistical performances of eigenstructure method, will find interesting material in (Kaveh and Brabell, 1986) and (Wang and Kaveh, 1986).

THE WIDE-BAND CASE

Seismic data are wide-band; to apply the narrow-band methods described above the data must be decomposed in frequency components, either by Fourier transform or by filtering with a bank of band-pass filters.

The results at different frequencies can be combined to yield a global result for the original wide-band estimation problem. This is because the number of wavefronts and the shape-parameters remain the same for all frequencies. The frequency components can be combined at different stages of the processing either by averaging the final estimates of the spectra (Wax et al., 1984), or by averaging the estimates of the covariance matrices of the different components. (Wang and Kaveh, 1985) In the later case, the frequency components must be linearly transformed to make the covariance matrices approximately *coherent* with each other. The rationale of this method is that averaging the covariance matrices increases the statistical robustness of the estimates. This is particularly important in the case

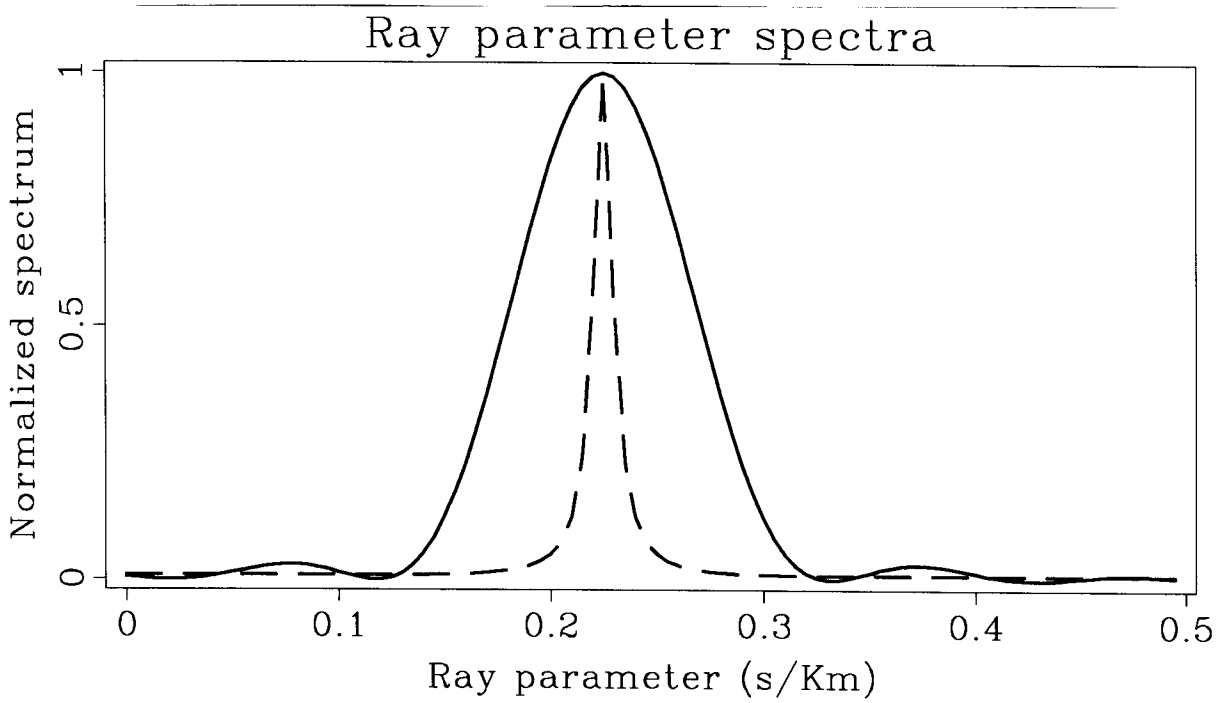

FIG. 5. Stacking spectrum (solid line) and eigenstructure spectrum (dashed line) for two monochromatic and fully correlated plane waves. Neither method resolves the two wavefronts.

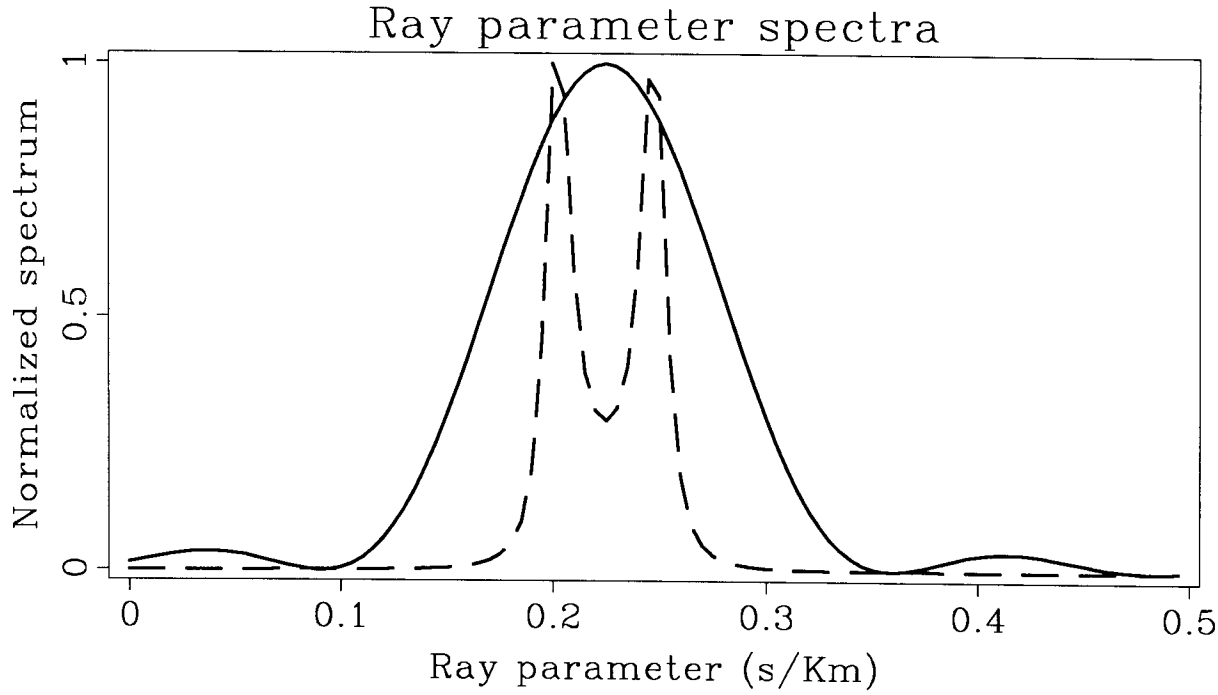

FIG. 6. Stacking spectrum (solid line) and eigenstructure spectrum (dashed line) for two monochromatic and fully correlated plane waves. Spatial smoothing is applied, and the eigenstructure spectrum resolves the two wavefronts.

of seismic reflections, when only few time samples can be used in the estimation of the covariance matrices. The disadvantage of combining the covariance matrices is that they are only approximately coherent.

In our computations, we combine both methods described above, averaging correlation matrices for nearby frequencies, and averaging spectra from different frequency bands.

At first, the data are time-corrected following the moveout $\tau(m,\bar{\theta})$; where $\bar{\theta}$ is an estimate of the shape parameter, obtained for instance by stacking spectrum analysis. The time correction renders the different frequency components of the wavefronts with shape parameters close to $\bar{\theta}$ more coherent. Before the time correction, the phase difference between two frequency components, with angular frequencies ω_1 and ω_2, and common shape parameter $\theta + d\theta$, is

$$\Delta\phi = (\omega_1 - \omega_2)\tau(m,\bar{\theta} + d\theta).$$

After the time correction the same phase difference becomes

$$\Delta\phi = (\omega_1 - \omega_2)\tau(m, d\theta).$$

(Our transformation for increasing the coherency between the frequency components is different from the one proposed by Wax and Kaveh).

The time corrected data are decomposed in few, and thus wide, frequency bands, using a bank of band-pass filters. The wider the frequency bands, the more robust the estimates of the covariance matrices. Robustness is gained at the expense of resolution, because the different frequency components inside each band are not completely coherent, even after the time correction.

To determine the number of wavefronts W impinging on the array of receivers, we select the value that minimizes the sum of the MDL criteria (Equation (12)) for each of the F frequency bands,

$$\sum_{f=1}^{F} MDL_f(W) = \sum_{f=1}^{F}[-2\log\left(\frac{\prod_{m=W+1}^{M}\hat{\lambda}_m(f)^{1/(M-W)}}{\frac{1}{M-W}\sum_{m=W+1}^{M}\hat{\lambda}_m(f)}\right)^{(M-W)T} + W(2M-W)\log(T)]. \quad (26)$$

Once the number of wavefronts W is determined, the shape parameter spectrum is obtained by averaging the parameter spectra of all the bands. For example the wide-band version of Equation (13a) is

$$P_{s1}(\theta) = \frac{1}{F}\sum_{f=1}^{F}\sum_{m=1}^{W} \mid \mathbf{a}(\theta,f)^H\hat{\mathbf{E}}_m(f) \mid^2. \quad (27)$$

If the signal to noise ratio in each band is known, the terms summed in Equations (26) and (27) could be weighted accordingly so as to increase the quality of the estimates.

The estimation of the covariance matrix from noisy data can be improved by *partial stacking*, that is summation of adjacent moveout-corrected traces. A further advantage of partial stacking is the reduction of the dimensions of the covariance matrix, and therefore also of the computational cost of the procedure. Partial stacking might have to be used in conjunction with spatial dip filtering to avoid aliasing of wavefronts with shape parameters significantly different from $\bar{\theta}$.

APPLICATION TO VELOCITY ANALYSIS

The wide-band method can be applied directly to a common-midpoint gather (CMP) for estimating higher resolution velocity-spectra. Velocity spectra are slightly different and more complicated than ray-parameter spectra. The properties of the steering vectors with the hyperbolic delays of Equation (3) are different from those of the steering vectors with the linear delays (Equation (2)). The differences are easily understood when the stacking spectrum of Figure 2 is compared to the corresponding stacking spectrum of Figure 7. Figure 7 shows the stacking spectrum for a monochromatic hyperbolic reflection with frequency 25 Hz and stacking slowness $\theta = .25$ s/Km. The arrays have 64 receivers spaced 20 m apart; the nearest offset is 40 m. The zero-offset time is 1 s. The spectrum has no true zeros because the steering vectors are never orthogonal. The main lobe is asymmetric, and wider toward lower stacking slownesses; the main lobe would have been wider for higher zero-offset times, and shorter nearest offset or lower stacking slownesses.

Figure 8 shows the synthetic CMP gather used to compare the performances of the eigenstructure method with the performances of the usual stacking method. Two hyperbolic reflections are recorded by an array of 64 geophones, spaced 20 m apart, with nearest offset of 40 m. The stacking slownesses are $\theta_1 = .2$ s/Km and $\theta_2 = .25$ Km/s; the zero-offset time is 1 s. The sources are wide-band, from 10 Hz to 50 Hz, correlated with correlation coefficient $\rho = .87$. The signal-to-noise ratio SNR is 2, with Gaussian white noise added. For testing the new method in more realistic situations, we applied random time shifts to the traces, drawn from a Gaussian distribution with standard deviation of 1 ms, and also increased the reflections amplitudes linearly with offset.

Figure 9 shows the stacking spectrum (solid line) and the eigenstructure spectrum (dashed line) for the data shown in Figure 8, computed at the correct zero-offset time of 1 s, and normalized to one. For the computation of the eigenstructure spectrum the data are decomposed in 6 frequency bands after applying time corrections corresponding to a stacking slowness $\bar{\theta} = .225$ s/Km, and reducing the number of traces to 8 by partial stacking. The results from the different frequency bands were combined following Equations (26) and (27). The eigenstructure spectrum has resolved well the two reflections while the stacking spectrum has not.

Figure 10 shows the stacking spectrum (solid line) and the eigenstructure spectrum (dashed line) when the stacking slownesses of the two reflections are $\theta_1 = .225$

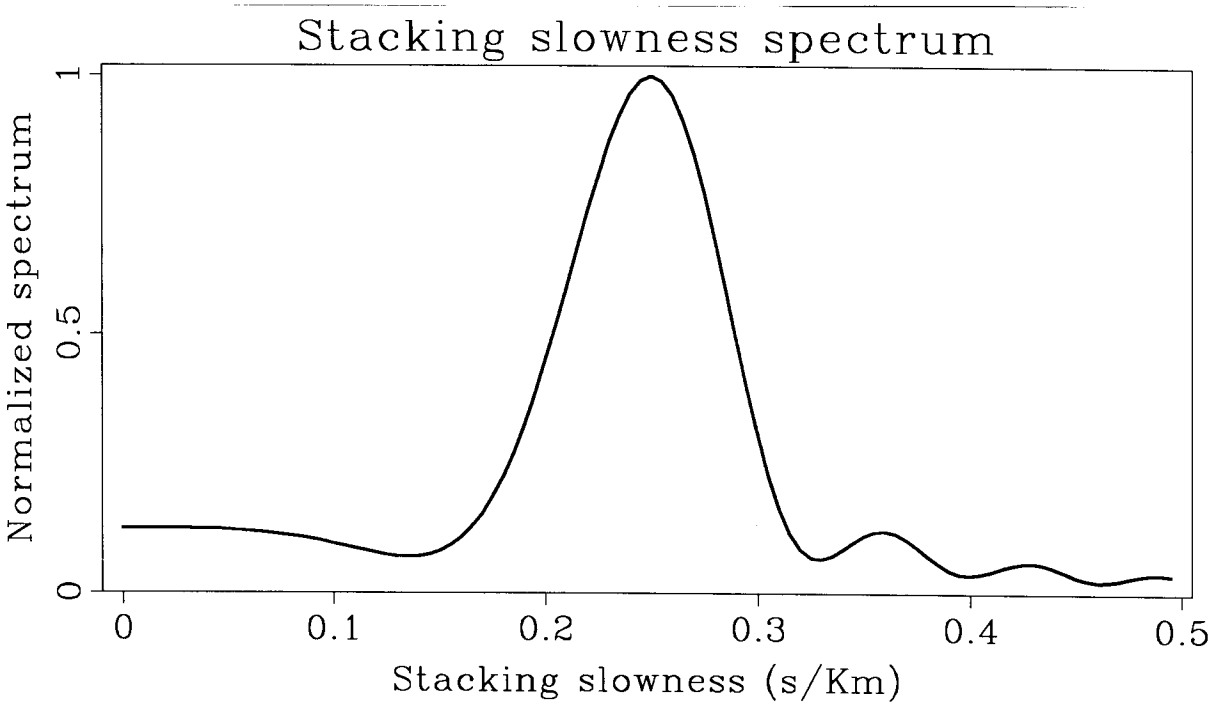

FIG. 7. Stacking spectrum for a monochromatic hyperbolic reflection with frequency 25 Hz and stacking slowness θ = .25 s/Km. The array has 60 receivers spaced 20m; and the zero-offset time is 1 s. The spectrum has no true zeros because the steering vectors are never orthogonal.

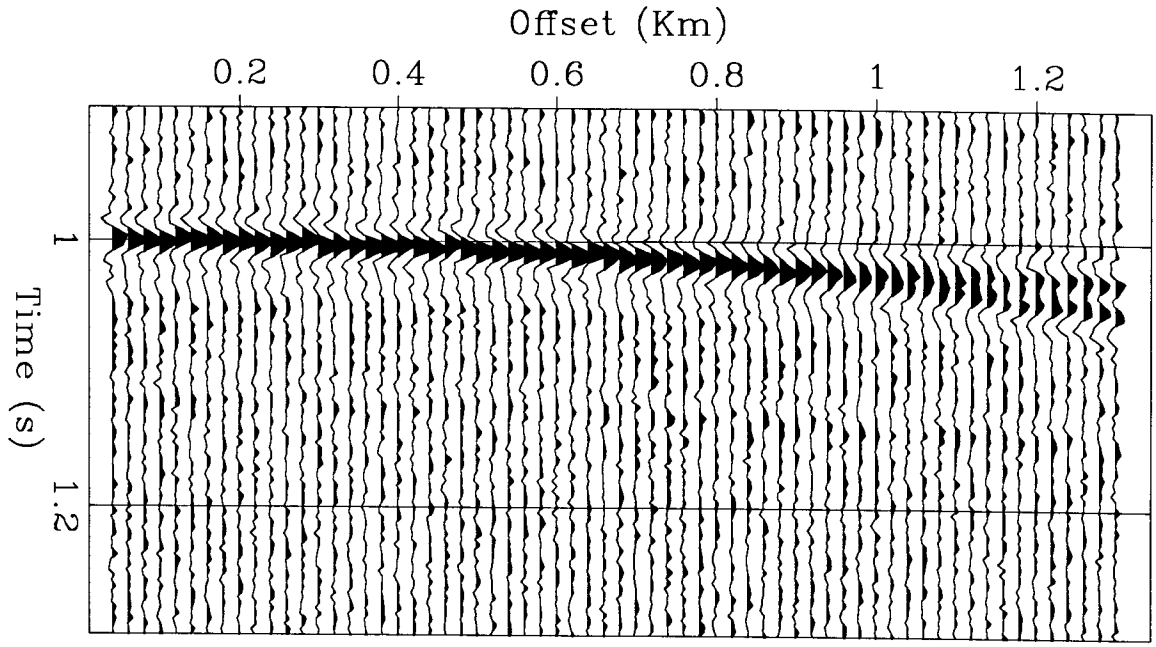

FIG. 8. Synthetic CMP gather used to compare the performance of the eigenstructure method with that of the stacking method. Two hyperbolic reflections are recorded with stacking slownesses θ_1 =.2 s/Km and θ_2 =.25 s/Km. The SNR of the data is 2. Random time shifts were applied to the traces.

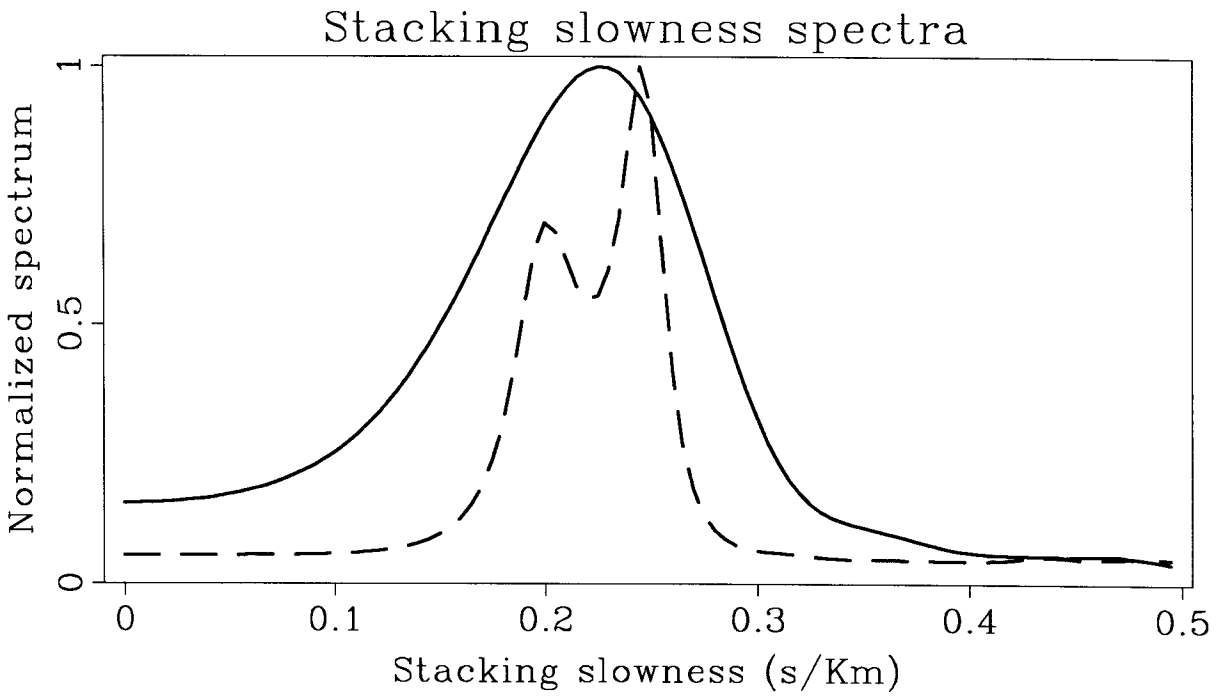

FIG. 9. The stacking spectrum (solid line) and the eigenstructure spectrum (dashed line) for the data shown in Figure 8. The eigenstructure spectrum has well-resolved the two reflections; the stacking spectrum has not.

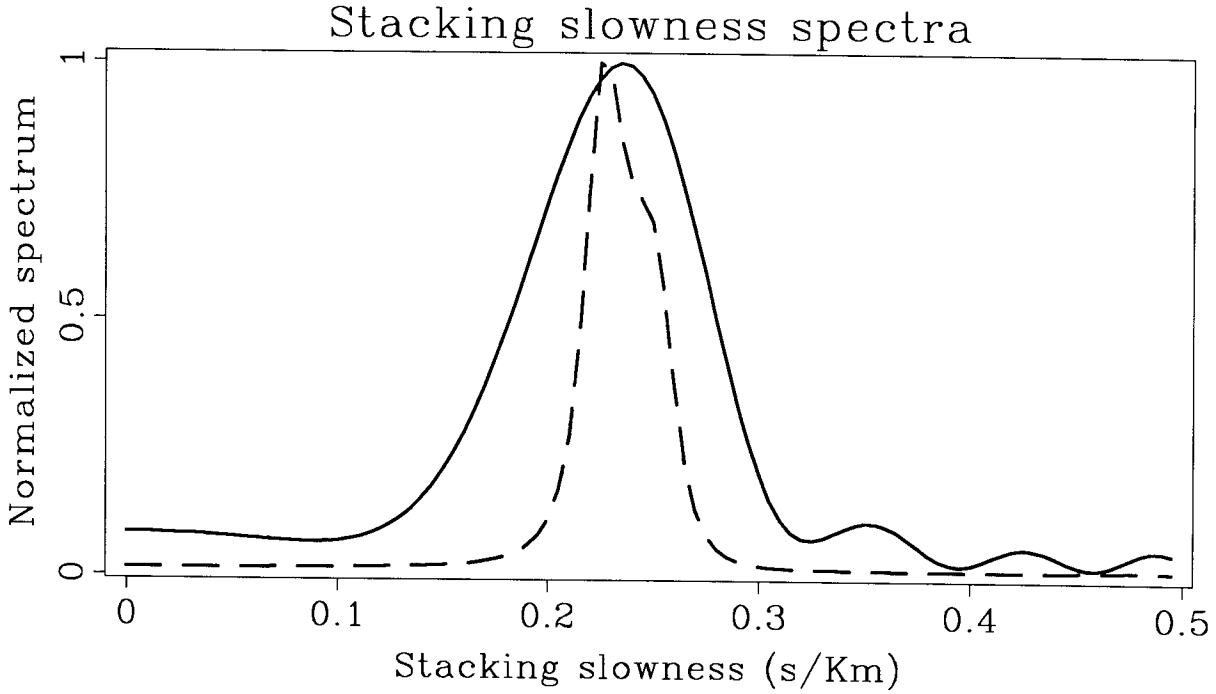

FIG. 10. The stacking spectrum (solid line) and the eigenstructure spectrum (dashed line) when the stacking slownesses of the two reflections are $\theta_1 = .225$ s/Km and $\theta_2 = .25$ s/Km. In this case, neither the eigenstructure, nor the stacking spectrum can resolve the two reflections.

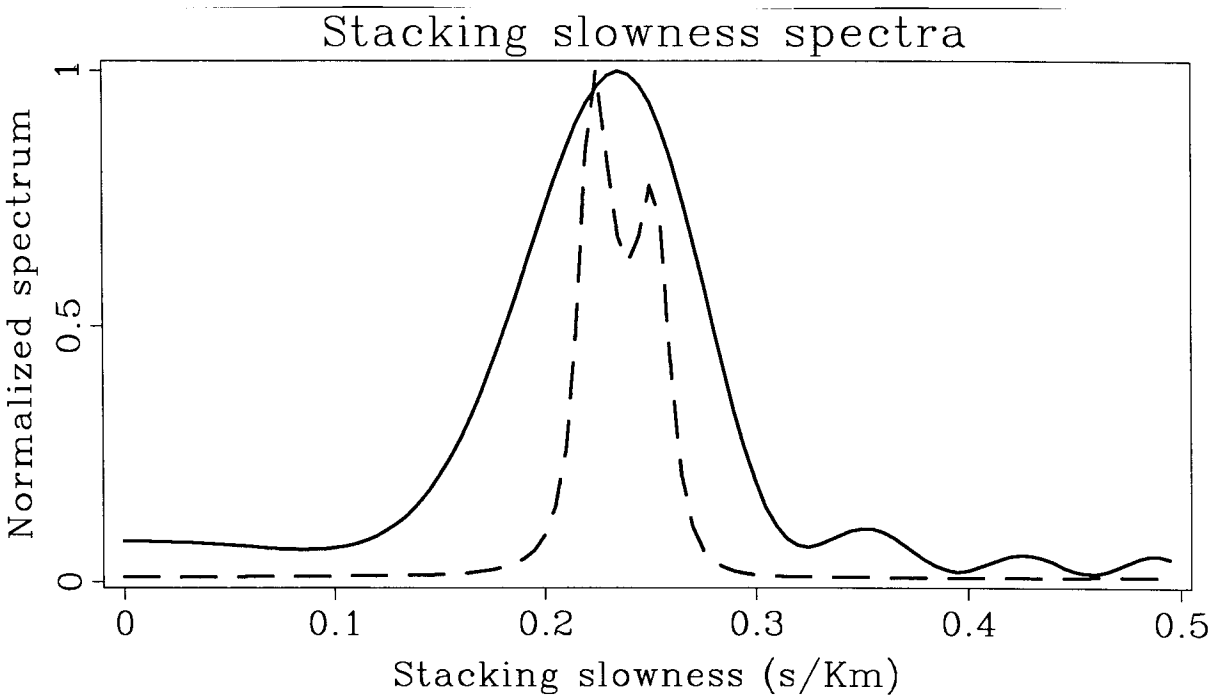

FIG. 11. The stacking spectrum (solid line) and the eigenstructure spectrum (dashed line) when the stacking slownesses of the two reflections are $\theta_1 = .225$ s/Km and $\theta_2 = .25$ s/Km, but the SNR is increased to 4. Now the eigenstructure spectrum can resolve the two reflections.

s/Km and $\theta_2 = .25$ s/Km, and the correlation coefficient between sources is $\rho = .6$. All other acquisition parameters are the same as for the data shown in Figure 8. In this case, also the eigenstructure spectrum fails to resolve the two reflections, because they are closer than before. However, if the SNR of the data is increased from 2 to 4, the eigenstructure spectrum can resolve the reflections, as shown in Figure 11. Both application of the eigenstructure method use partial stacking with a shape parameter $\bar{\theta} = .237$.

APPLICATION TO LOCAL SLANT STACKS

Using shape-parameter spectra, we implicitly assume that the data can be modeled by a simple propagation model; either as plane waves or as hyperbolic reflections. These simple models predict well the data locally, but they are not accurate when used to model data recorded over a larger area (a cable length). On a larger scale, the rocks cannot be considered homogeneous. Furthermore, in the decomposition of hyperbolic reflections in local plane waves, the plane wave model is valid only in the Fresnel zone of the reflections. There are thus two conflicting needs: shorter arrays for accuracy of the model and spatial resolution of the estimates, versus longer arrays for shape-parameter resolution. The eigenstructure spectrum allows using shorter arrays than the stacking spectrum, without decreasing the res-

olution of the estimates. Therefore, high-resolution spectra can prove crucial to the success of a local spectra estimation method.

Synthetic example

The following example illustrates that the eigenstructure spectrum succeeds in resolving two reflections at their intersection point. The stacking spectrum cannot resolve the two reflections, because of the limited width of the Fresnel zone. Figure 12 shows a synthetic CMP gather with two reflections – a primary with stacking velocity 2.6 Km/s, and a multiple with stacking velocity 1.8 Km/s. There are 60 geophones, spaced 20 m apart; the nearest offset is 20 m. The frequency band of the sources is 20-50 Hz; the sources are correlated with correlation coefficient $\rho = .8$. The SNR is 2 with Gaussian white noise added. Random time shifts drawn from a Gaussian distribution with standard deviation of 1 ms are applied to the traces.

Figure 13 shows the normalized local ray parameter spectra, computed at the intersection of the two reflections, using a reduced array of 20 geophones. The width of the reduced array is approximately the width of the Fresnel zone of the reflections. The dotted line has two spikes at the correct values of the ray parameters. The dashed line is the eigenstructure spectrum; the solid line is the stacking spectrum. The eigenstructure spectrum is computed by decomposing the data in 6 frequency bands, after applying a time correction, corresponding to the ray parameter $\bar{\theta} = .12$ s/Km, and partial stacking that reduces the number of traces to 5. Spatial smoothing is used to *uncorrelate* the sources, subdividing the array in 2 subarrays. Only the eigenstructure method resolves the two reflections and estimates their ray parameters fairly well. The Fresnel zone is too narrow for the stacking spectrum to resolve the reflections.

Field-data example

The advantages of the eigenstructure method are confirmed by its application to the marine CMP gather shown in Figure 14. We estimate local spectra at the intersection point of a primary reflection and of a water-bottom multiple. In Figure 14 the region of interference between the two reflections is indicated by a balloon. The gather belongs to a line donated to SEP by British Petroleum and already used by Fowler (1986) to test his migration velocity analysis method. The data sampling rate is 2 ms in time and 32 m in the offset dimension.

The broad frequency spectrum of the data, extending up to 100 Hz, allows the comparison of stacking spectra versus eigenstructure spectra for different frequency band-widths. As expected the stacking spectrum cannot resolve the two reflections when the data frequency is too low. Further, we varied the length of the subarray used for estimating local spectra in order to study the trade-off between ray-parameter resolution and spatial resolution of the local estimates. The results show that the eigenstructure method has a higher spatial resolution than the stacking method.

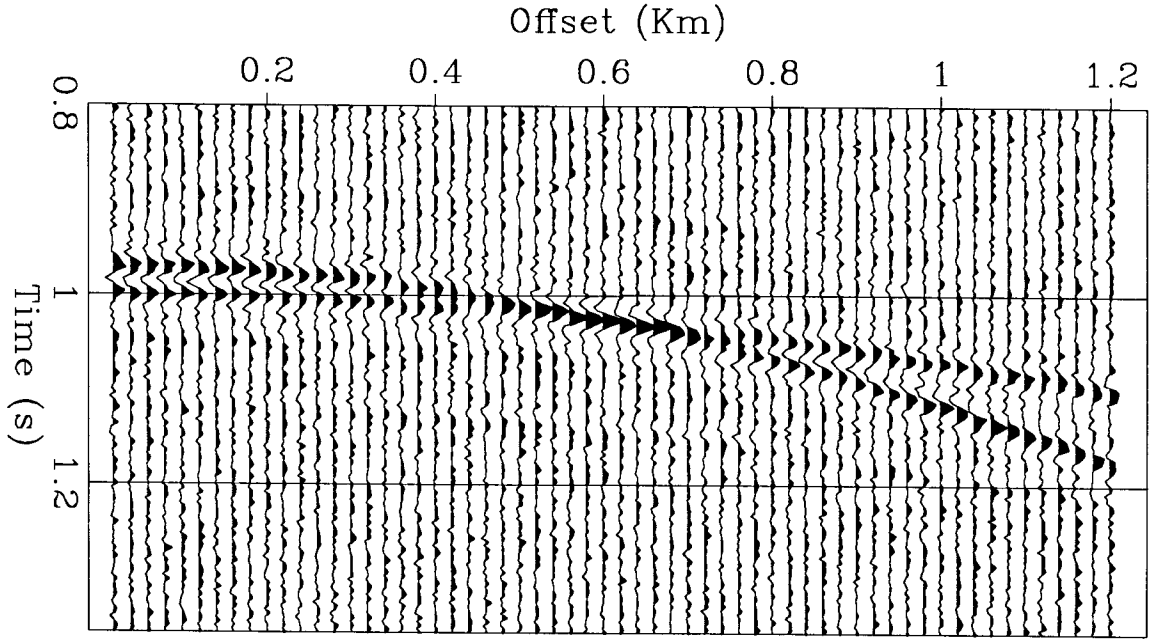

FIG. 12. A synthetic CMP gather. The stacking velocity of the primary reflection is 2.6 Km/s; the stacking velocity of the multiple reflection is 1.8 Km/s. The goal is to resolve the two reflections at their intersection point, using ray-parameter spectra.

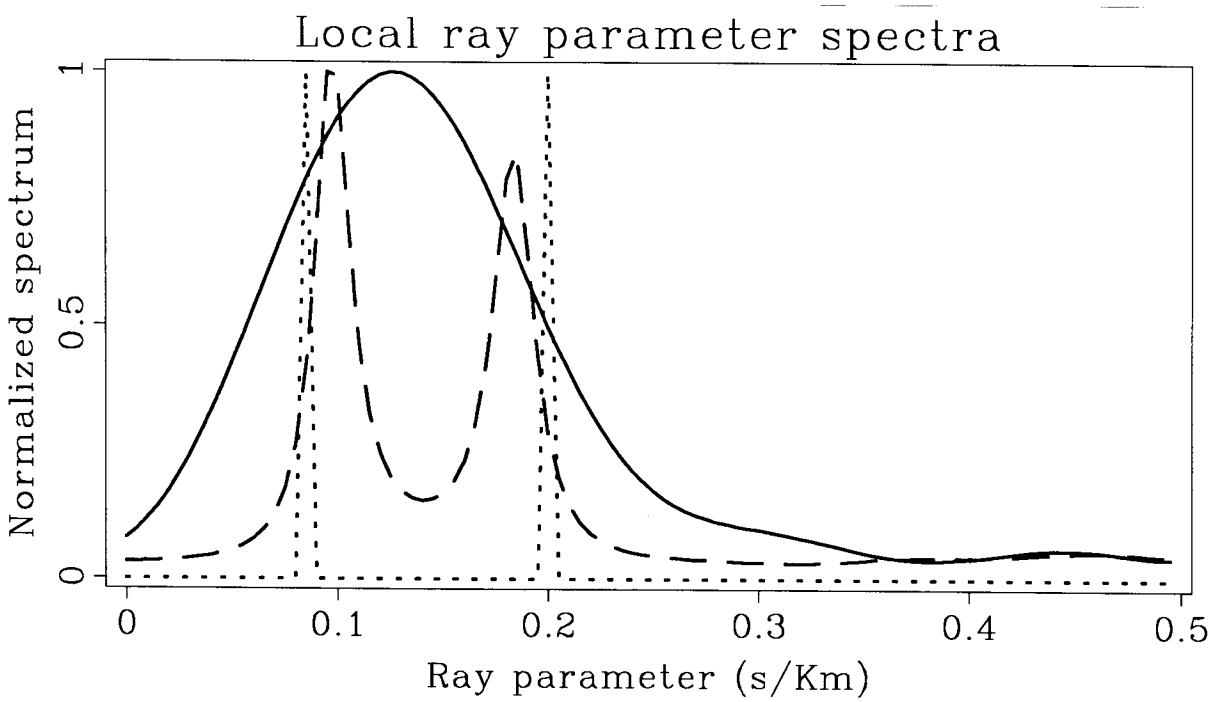

FIG. 13. Normalized local ray parameter spectra, computed at the intersection of the two reflections. The dotted line has two spikes at the correct values of the ray parameters. The dashed line is the eigenstructure spectrum; the solid line is the stacking spectrum. Only the eigenstructure method resolves the two reflections and estimate their ray parameters fairly well.

Figure 15 shows the normalized ray parameter spectra estimated from the original gather with bandwidth from 15 Hz to 100 Hz. A subarray of 8 geophones, centered at the intersection point of the two reflections, is used for the estimation. As reference values we used the reflections ray parameters estimated by hand from a plot of the gather; even if carefully measured these values are affected by some error. In all the remaining figures the dotted line has two spikes at the reference values of the ray parameter. The dashed line is the eigenstructure spectrum; the solid line is the stacking spectrum. The eigenstructure spectrum is computed by decomposing the data in 10 frequency bands, after applying a time correction, corresponding to the ray parameter $\bar{\theta}$=.32 s/Km. The stacking spectrum is computed using semblance as a coherency measure along the offset direction. Both methods resolve the two reflections. The maxima of the spectra are approximately in agreement with the ray parameter values estimated by hands.

Figure 16 shows the results obtained by decreasing the number of traces used in the computation of the local spectra from 8 to 6. The purpose of using a shorter subarray is to increase the spatial resolution of the local estimates. Only the eigenstructure spectrum resolves the two reflections; the subarray is too short for the stacking spectrum.

The resolution of local spectra depends also on the frequency band-width of the data. Therefore, we compute the spectra after having band-passed the gather with different high-frequency cut-off values. Figure 17 shows the local spectra computed from a gather with bandwidth from 15 Hz to 33 Hz and using a subarray of 8 geophones. The eigenstructure spectrum is computed by decomposing the data in 4 frequency bands, after applying a time correction, corresponding to the ray parameter $\bar{\theta}$=.32 s/Km. The eigenstructure spectrum (dashed line) resolves both reflections well, while the stacking spectrum (solid line) misses the primary reflection. The eigenstructure spectrum (dashed line) is also successful in resolving both reflections when using a subarray of only 6 geophones (Figure 18). The stacking spectrum, as expected, fails in this extreme situation.

CONCLUSIONS

The velocity spectra, or ray parameter spectra, obtained using the proposed method have higher resolution than the spectra obtained using the classical stacking method. The field-data example and the synthetic examples show the utility of the high-resolution methods for some practical applications. In particular the field-data example shows the gain in lateral resolution that can be achieved in the estimation of local spectra using the new eigenstructure method.

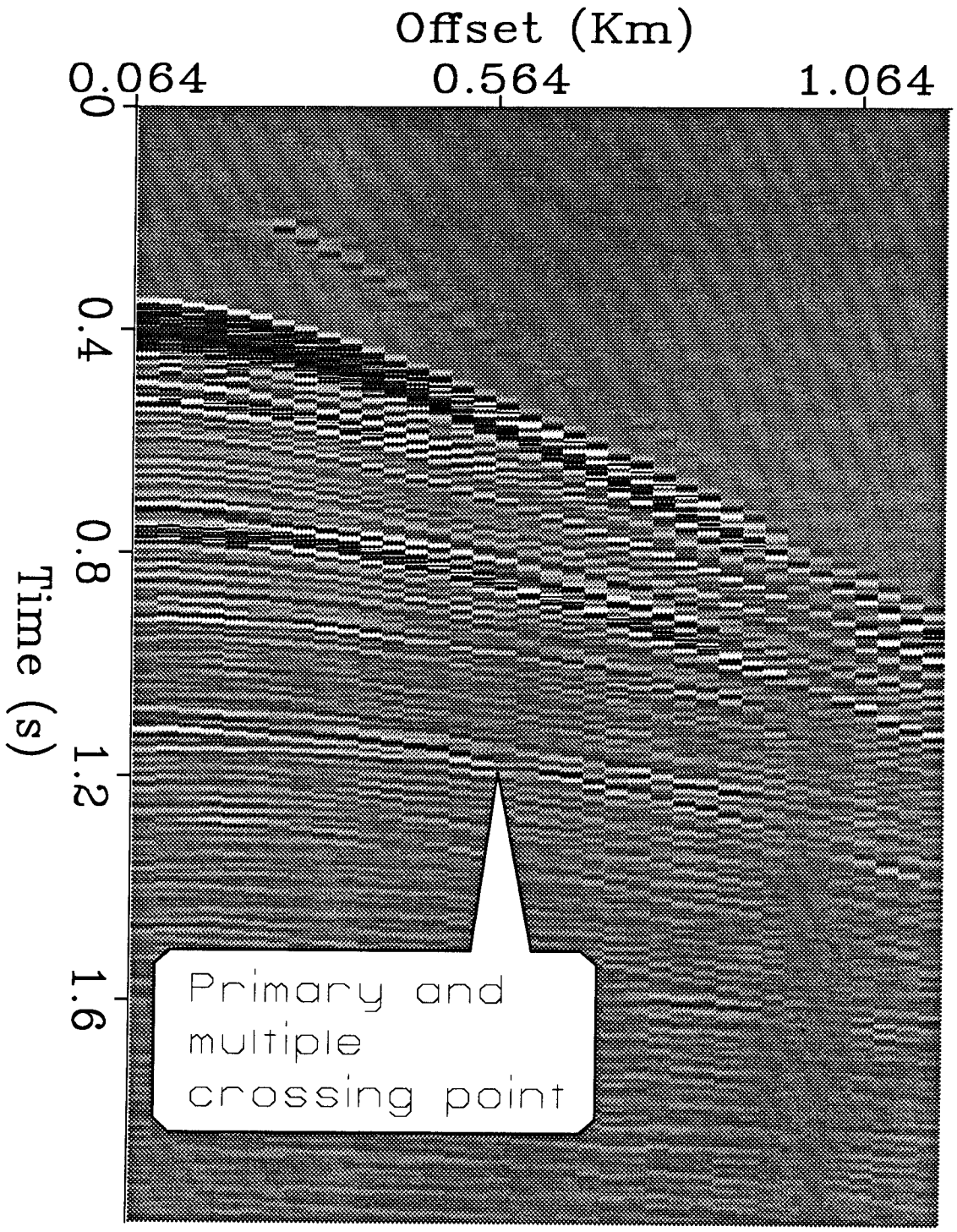

FIG. 14. A marine CMP gather donated to SEP by British Petroleum. We estimate local spectra at the intersection point between a primary reflection and a water-bottom multiple; in the region indicated by the balloon.

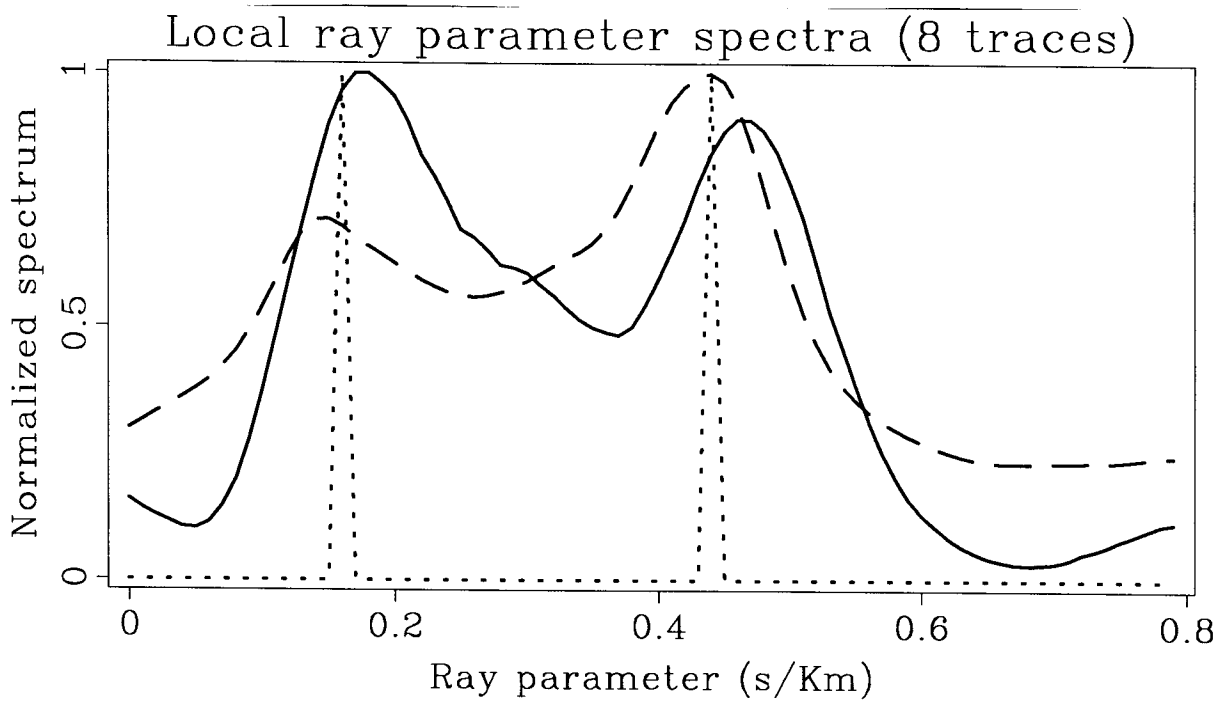

FIG. 15. Normalized local ray parameter spectra. The dashed line is the eigenstructure spectrum; the solid line is the stacking spectrum. The dotted line has two spikes at the values of the ray parameter estimated by hand. The data bandwidth is from 15 Hz to 100 Hz. A subarray of 8 geophones is used. The maxima of the spectra are approximately in agreement with the ray parameter values estimated by hands.

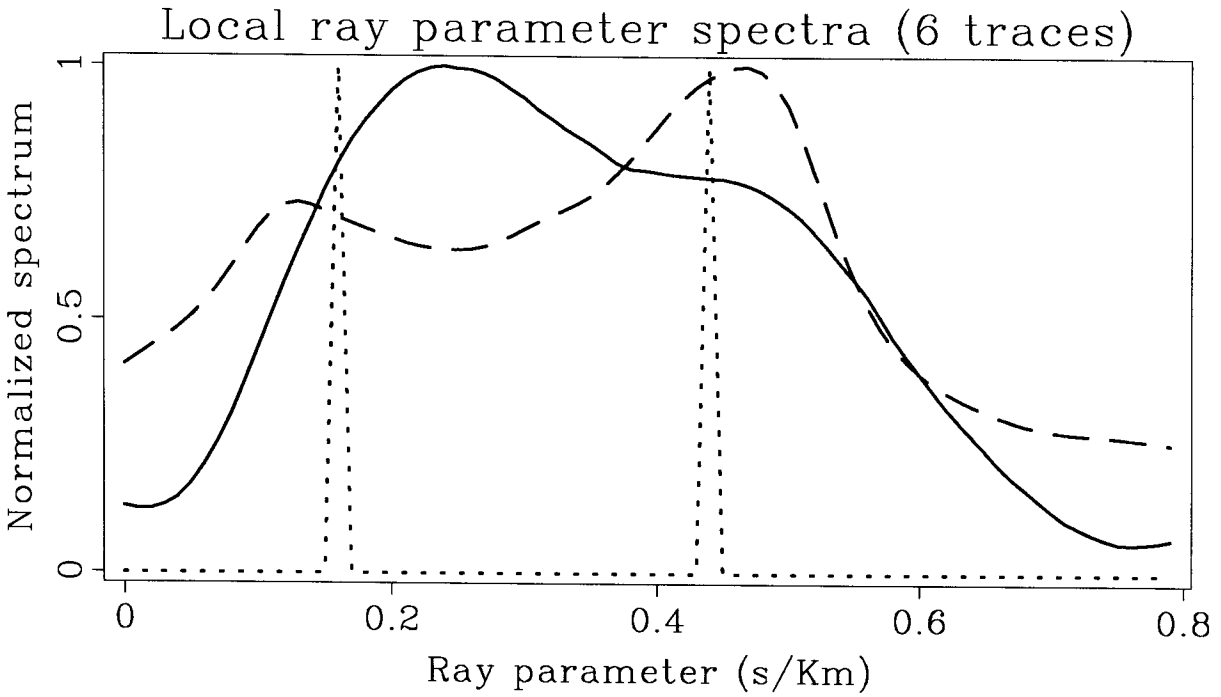

FIG. 16. The stacking spectrum (solid line) and the eigenstructure spectrum (dashed line) when a subarray of only 6 geophones is used. Only the eigenstructure spectrum can resolve the two reflections; the subarray is too short for the stacking spectrum.

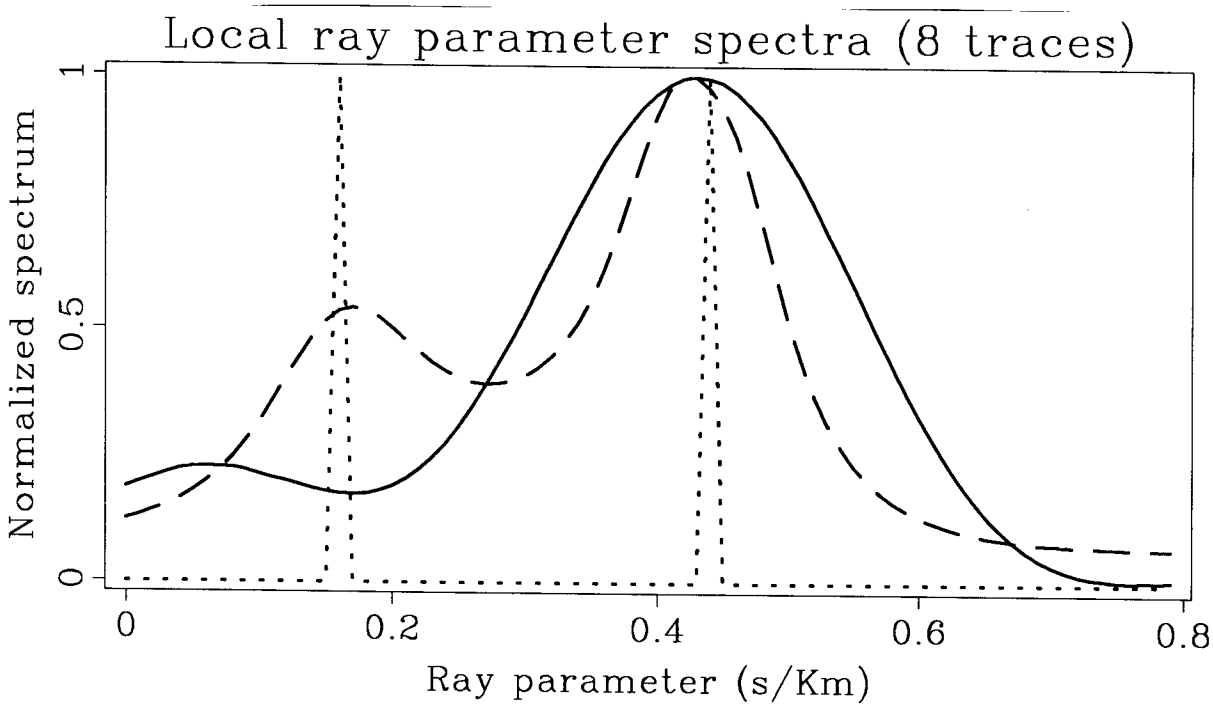

FIG. 17. The stacking spectrum (solid line) and the eigenstructure spectrum (dashed line) when the data bandwidth is from 15 Hz to 33 Hz, and a subarray of 8 geophones is used. Only the eigenstructure spectrum can resolve the two reflections; the data frequency is too low for the stacking spectrum.

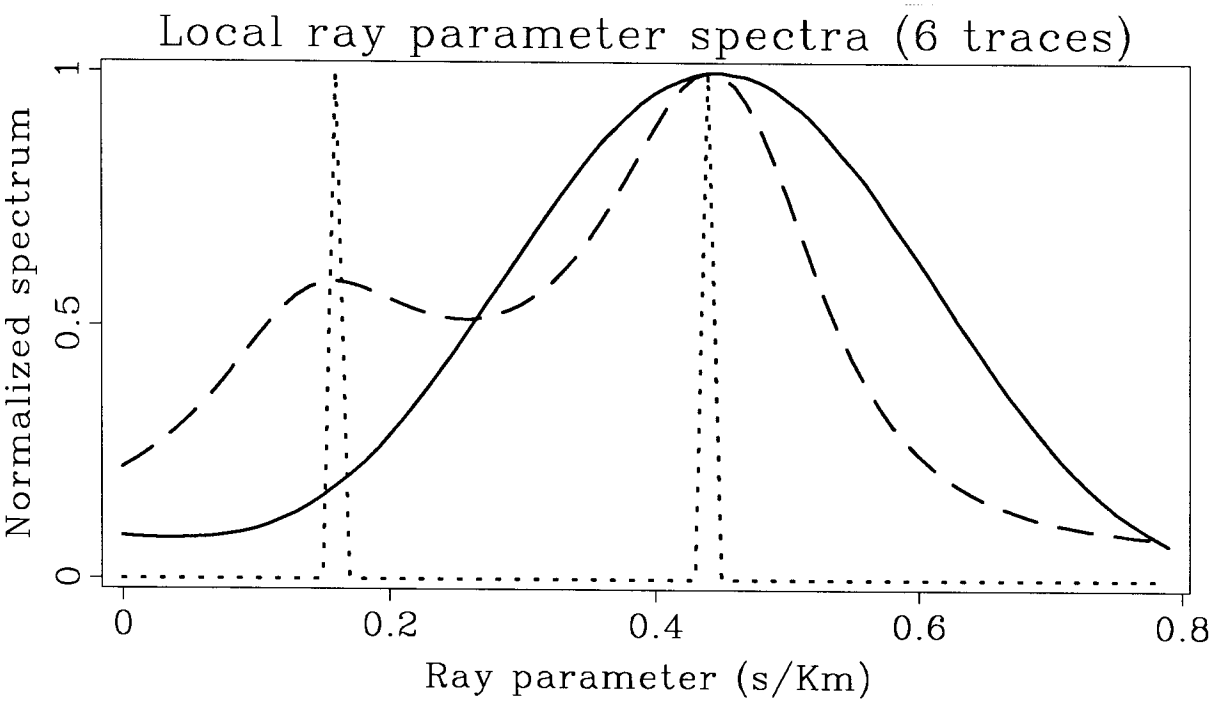

FIG. 18. The stacking spectrum (solid line) and the eigenstructure spectrum (dashed line) when the data bandwidth is from 15 Hz to 33 Hz, and a subarray of 6 geophones is used. The eigenstructure spectrum can resolve the two reflections even in this extreme situation.

ACKNOWLEDGMENTS

We would like to thank Fabio Rocca for challenging us to improve our understanding of the subject by asking questions that are simple in the formulation, but hard to answer.

We also would like to thank British Petroleum for making available to SEP the field data we used.

REFERENCES

Akaike, H., 1973, Information theory and an extension of the maximum likelihood principle : Proc. 2nd Int. Symp. Inform. Theory, suppl. Problems of Control and Inform. Theory: 267–281.

Anderson, T.W., 1963, Asymptotic theory for principal component analysis: Ann. J. Math. Stat., **34**, 122–148.

Bienvenu, G., Kopp, L., 1983, Optimality of high resolution array processing using the eigensystem approach: IEEE Trans. Acoust. Speech, Signal Processing, **31**, 1235–1248.

Claerbout, J.F., 1976, Fundamentals of geophysical data processing: McGraw-Hill Inc..

Fowler, P., 1986, Migration velocity analysis: preliminary data tests: SEP – **50**, 139–150.

Kaveh, M., and Barbell, A., 1986, The statistical performance of the MUSIC and the minimum-norm algorithms in resolving plane waves in noise: IEEE Trans. Acoust. Speech, Signal Processing, **34**, 331–341.

Kostov, C., and Biondi, B., 1987, Improving resolution of slant stacks using beam stacks; paper presented at the 57th Annual International SEG Meeting, New Orleans, LA.

Rissanen, J., 1978, Modeling by shortest data description: Automatica, **14**, 465–471.

Schmidt, R., 1986, Multiple emitter location and signal parameter estimation: IEEE Trans. Antennas Propagat., **34**, 276–280.

Shan, T.J., Paulraj, A., and Kailath, T., 1987, On smoothed rank profile tests in eigenstructure methods for detection-of-arrival estimation IEEE Trans. Acoust. Speech, Signal Processing, **35**, 1377–1385.

Shan, T.J., Wax, M., and Kailath, T., 1985, On spatial smoothing for direction-of-arrival estimation of coherent signals: IEEE Trans. Acoust. Speech, Signal Processing, **33**, 806–811.

Sguazzero, P., and Vesnaver, A., 1987, A comparative analysis of algorithms for stacking velocity estimation: Proc. of the workshop on Deconvolution and Inversion, Rome, Italy.

Sword, C.H., 1987, Tomographic determination of interval velocities from reflection seismic data: The method of controlled directional reception: Ph.D. thesis, Stanford University.

Taner, M.T., and Koehler, F., 1969, Velocity spectra-digital computer derivation and applications of velocity functions: Geophysics, **34**, 859–881.

Wang, H., and Kaveh, M., 1985, Coherent signal-subspace processing for the detection and estimation of angles of arrival of multiple wide-band sources: IEEE Trans. Acoust. Speech, Signal Processing, **33**, 823–831.

Wang, H., and Kaveh, M., 1986, On the performance of signal-subspace processing Part 1: Narrow band systems: IEEE Trans. Acoust. Speech, Signal Processing, **34**, 1201–1209.

Wax, M., and Kailath, T., 1985, Detection of signals by information theory criteria: IEEE Trans. Acoust. Speech, Signal Processing, **33**, 387–392.

Wax, M., Shan, T.J., and Kailath, T., 1984, Spatio-temporal spectral analysis by eigenstructure methods: IEEE Trans. Acoust. Speech, Signal Processing, **32**, 817–827.

Антигуманная идеология современного капитализма наносит все больший ущерб духовному миру людей.

–Из Программы КПСС

The anti-human ideology of contemporary capitalism causes more and more damage to people's spiritual world.

–From the Program of the CPSU

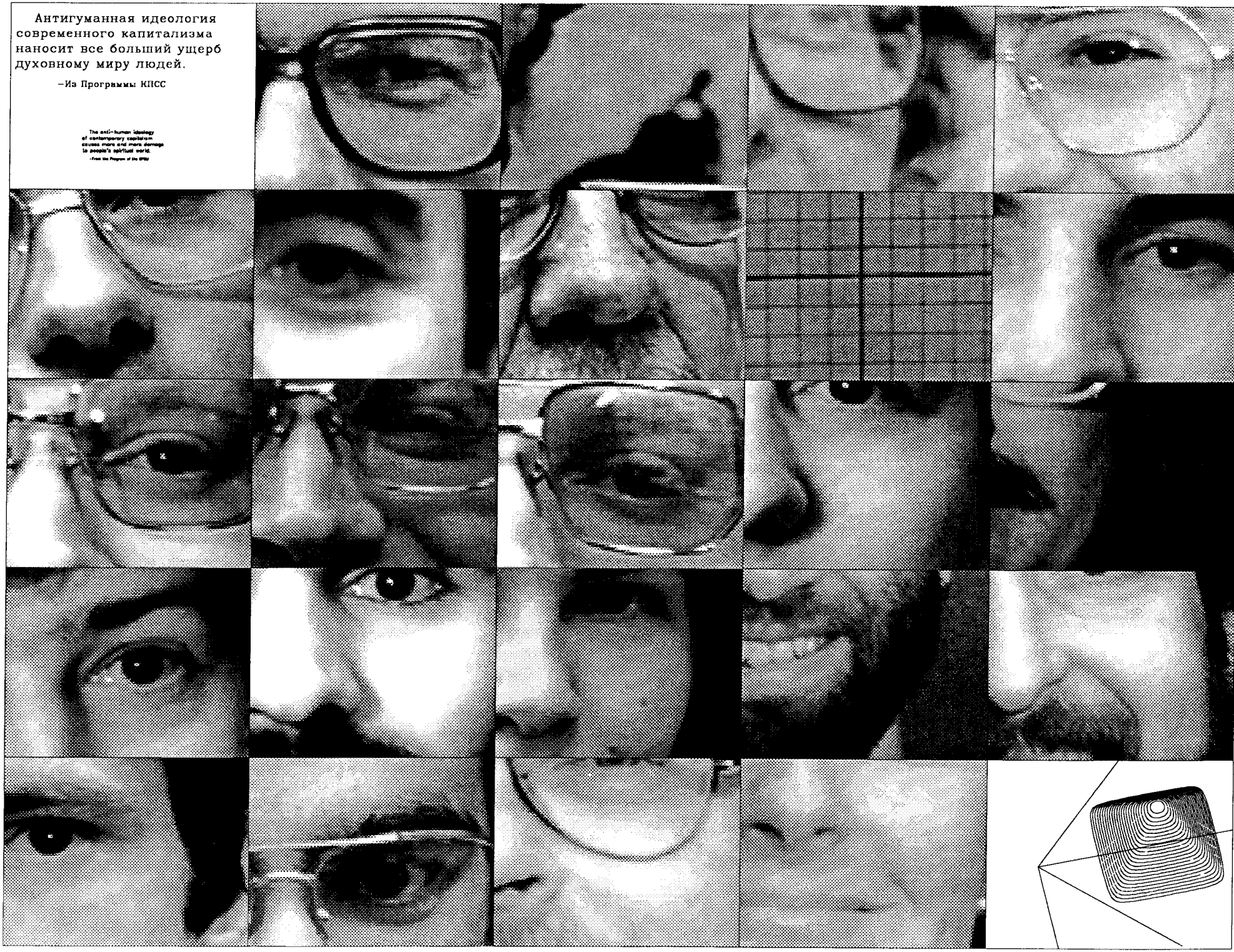

SEE PAGE 206 FOR CODE